AIAA JOURNAL
Vol. 32, No. 4, April 1994

Aeroelastic Response of Composite Rotor Blades Considering Transverse Shear and Structural Damping

Sung Nam Jung* and Seung Jo Kim†
Seoul National University, Seoul 151-742, Republic of Korea

The effects of transverse shear deformations and structural damping on the flutter phenomena of a composite rotor blade in hover have been investigated using the finite element method. First-order shear deformation theory with rotary inertia effects and a damped element model of composite laminates are employed for the structural formulation. A quasisteady aerodynamic theory with a dynamic inflow model is used. Torsion-related out-of-plane warping and noncirculatory aerodynamic components are also incorporated in the formulation. Using these structural and aerodynamic tools, several numerical studies are carried out, first to validate the current approach and second to show the effects of transverse shear deformations and structural damping on the aeroelastic stability of a composite rotor as a function of fiber orientation. The predictions derived by the frequency analysis of this model are found to be more accurate than those given by an alternative approach compared with experimental data. It is shown that the transverse shear flexibility tends to lower the frequency of the rotor, and generally has a destabilizing effect on the lag mode and a stabilizing effect on the flap mode. It is also presented that the magnitude of structural damping can be controlled by changing ply orientation angle.

Nomenclature

C_T	=	rotor thrust coefficient
c_d	=	blade section drag coefficient
c_l	=	blade section lift coefficient
EA	=	effective extensional stiffness
E_{11}	=	longitudinal Young's modulus
E_{22}	=	transverse Young's modulus
G_{12}, G_{13}	=	shear modulus
h, b	=	height and width of box section, respectively
k_m	=	mass radius of gyration of blade cross section = $\sqrt{k_{m1}^2 + k_{m2}^2}$
k_{m1}, k_{m2}	=	principle mass radii of gyration of blade cross section
m	=	mass per unit length of the blade
R	=	blade length
t_h, t_v	=	wall thickness in horizontal and vertical layers, respectively
x, y, z	=	undeformed blade coordinates
β_{pc}	=	precone angle
ε_{xx}, $\varepsilon_{x\eta}$, $\varepsilon_{x\zeta}$	=	engineering strain components
Λ_H, Λ_V	=	ply angle in horizontal and vertical laminates, respectively
ξ, η, ζ	=	deformed blade coordinates
ρ	=	mass per unit volume
σ_{xx}, $\sigma_{x\eta}$, $\sigma_{x\zeta}$	=	engineering stress components
$\hat{\phi}$	=	geometric twist
Ω	=	rotor speed
$(\,)'$	=	d/dx
$(\dot{})$	=	d/dt

Introduction

THE advanced composite materials have been widely used in the aerospace applications due to their high stiffness-to-weight and high strength-to-weight ratios, which have a great potential for reducing structural weight. However, the analysis of composite structures is a complex task due to the existence of coupling stiffness. Furthermore, it has been pointed out that nonclassical structural effects, such as transverse shear and warping, have a considerable influence on the static and dynamic behavior of a laminated structure compared to that of a homogeneous isotropic structure, since the composites have a very low transverse shear modulus compared to in-plane tensile moduli.[1,2] Therefore, appropriate analytical tools for capturing these nonclassical effects are required to accurately predict the composites behavior. Recently, numerous analytical studies have been reported, which can take into account the nonclassical effects of composite beams, but to date, only a few studies have been conducted on the aeroelastic response of a composite rotor blade.

Hong and Chopra[3] extended the work of Hodges and Dowell[4] to demonstrate the effect of fiber orientation on the aeroelastic stability boundary. They used a simplified beam model, in which the transverse shear flexibility was not included in the formulation, but provided a fundamental basis on the flap-lag-torsion aeroelastic analysis of a composite rotor blade. Rand[5] studied the theoretical modeling of the linear periodic response of thin-walled composite helicopter rotor blades in forward flight. The formulation allows the determination of a detailed description of both torsional- and bending-related warping displacements. A recent finite element formulation for the aeroelastic response, vibratory blade, and hub loads of a helicopter with elastically tailored composite rotor blades was presented by Smith and Chopra,[6] wherein a shear-flexible 19-DOF beam element was used. The strain-displacement relations of Hodges and Dowell were modified to include the effects of transverse shear deformations. As a result, additional sectional constants associated with the transverse shear deformations appeared in the strain energy expression. Both the transverse shear deformations and the bending deformations were assumed to have the same order of magnitude. Calculated values of the rotating natural frequencies of coupled composite box beams were compared with other results, and they showed that the correlation between these results is generally within 5–10% error bounds.

In the present work, a finite element method is applied for the aeroelastic stability analysis of a composite rotor blade

Received April 6, 1993; revision received Aug. 31, 1993; accepted for publication Sept. 25, 1993.

*Graduate Research Assistant, Department of Aerospace Engineering.

†Associate Professor, Department of Aerospace Engineering. Member AIAA.

idealized as a laminated thin-walled box beam. The nonlinear differential equations of motion for the finite element model are obtained by using Hamilton's principle. Quasisteady aerodynamic theory is used to evaluate aerodynamic forces, and a dynamic induced inflow model of Pitt and Peters[7] is introduced to account for unsteady aerodynamic effects. Noncirculatory-origin aerodynamic components are also included. In the finite element model, twenty-three degrees of freedom per element, including eight transverse shear degrees of freedom, were developed to fully consider the flap-lag-torsion behavior of a composite blade. In considering transverse shear deformations, the present research differs from that of Ref. 6 in that different degrees of freedom and different ordering schemes ($\varepsilon^{3/2}$ order is assumed for the magnitude of transverse shear deformations.) are used to perform aeroelastic analysis of a composite rotor blade in an effective manner. The method for including transverse shear flexibility in the analysis of composite beams was adopted from the work of Chen and Yang,[8] which included shear deformations by dividing the total transverse displacement into the displacement due to bending and the displacement due to transverse shear deflection. As a result, the aerodynamic forces and moments induced by the blade motion are also the sum of the forces and moments induced by bending deformation and transverse shear deformation. In order to consider the sectional distribution of shear stresses in a simple manner, the formula of the shear correction factors for the thin-walled box section developed by Cowper[9] was used. Rotary inertia effects due to the rotation of the cross section are also considered in the formulation.

In general, materials with high stiffness have low damping while materials with high damping have low stiffness. However, the advanced composite materials have not only high stiffness but also high damping characteristics since high stiffness can be obtained from fiber material and high damping from matrix material.[10] This in turn results in an anisotropic nature to be analyzed thoroughly in the structural damping behavior of a composite structure. Thus the statement, "The composites must be treated as composites,"[3] can also be emphasized in the analysis of structural damping for the composite rotor. In this work, the damped element model presented in Lin et al.[11] is incorporated in the formulation to determine the vibrational damping parameters such as modal damping ratios.

Using the aforementioned shear deformable beam finite elements along with the damped element model, this study aims at construction of a more enhanced aeroelastic analysis of composite rotor blades.

Formulation

Consider a laminated composite box beam rotating with constant angular velocity Ω, as shown in Fig. 1. This is a simplified model of a composite rotor blade. Each lamina made of unidirectional fiber-reinforced material is assumed to be homogeneous orthotropic. The orthotropic axes of lamina may be oriented at an arbitrary angle with respect to the beam axis (Fig. 1). A Cartesian coordinate system (x, y, z) is attached to the undeformed blade which is at a precone of β_{pc}, the x-axis coincides with the elastic axis, and the y-axis is in the plane of rotation (Fig. 1). The orthogonal coordinate system (ξ, η, ζ) is attached to the deformed blade such that the ξ-axis is tangential to the deformed elastic axis and the (η, ζ) axes are the principal axes of the cross section. The deformation of the blade in space is described by the displacements u, v, and w measured along the undeformed elastic axis. The u, v, and w are, respectively, the axial, lead-lag, and flap elastic deflections. The transverse shear deformations are included in the present formulation by splitting the transverse displacements of lag and flap bending into two parts as

$$\begin{aligned} v &= v_b + v_s \\ w &= w_b + w_s \end{aligned} \tag{1}$$

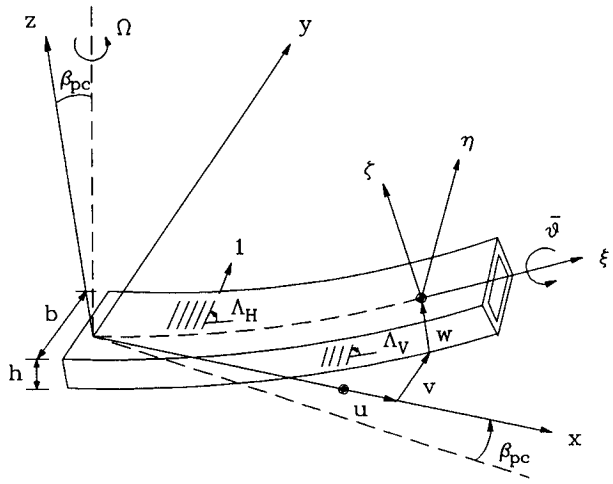

Fig. 1 Composite box beam geometry and deflections.

where the subscript b represents bending deformation and the subscript s shear deformation. The attitude of the cross section is described with the use of three Euler angles. The present analysis uses the lag-flap-pitch sequence of rotations defined in Ref. 4. The Euler third angle $\bar{\theta}$ is written as

$$\begin{aligned} \bar{\theta} &= \theta_0 + \hat{\phi} \\ \hat{\phi} &= \phi - \int_0^x v_b'' w_b' \, dx \end{aligned} \tag{2}$$

where θ_0 is the blade pretwist, $\hat{\phi}$ the geometric twist, and ϕ the elastic twist due to torsion. The transformation relationships between the undeformed coordinates (x, y, z) and the deformed coordinates (ξ, η, ζ) are given in Ref. 4.

In deriving the equations of motion for the composite blade, an ordering scheme is used as in Ref. 4. That is, if the largest terms of the energy expression are $\mathcal{O}(\varepsilon^4)$, then all terms of $\mathcal{O}(\varepsilon^4)$ and $\mathcal{O}(\varepsilon^5)$ are retained (e.g., first- and second-order terms), and generally $\mathcal{O}(\varepsilon^6)$ are discarded with the exception of some third-order terms related to torsion equation. It is assumed that transverse shear deformations v_s and w_s are of order $\varepsilon^{3/2}$ compared to bending deformations, v_b and w_b of order ε, and the other field variables of the same order of magnitude as described in Ref. 4.

The nonlinear strain-displacement relations for small strains and moderately large deformations, up to second order, are written in terms of displacement derivatives in the following form:

$$\begin{aligned} \varepsilon_{xx} &= u' + \frac{v_b'^2}{2} + \frac{w_b'^2}{2} - \lambda_T \phi'' + (\eta^2 + \zeta^2) \\ &\times \left(\theta_0' \phi' + \frac{\phi'^2}{2}\right) - v_b''\{\eta \cos(\theta_0 + \hat{\phi}) - \zeta \sin(\theta_0 \\ &+ \hat{\phi})\} - w_b''\{\eta \sin(\theta_0 + \hat{\phi}) + \zeta \cos(\theta_0 + \hat{\phi})\} \\ \gamma_{x\eta}' &= -\left(\zeta + \frac{\partial \lambda_T}{\partial \eta}\right) \phi' \\ \gamma_{x\zeta}' &= \left(\eta - \frac{\partial \lambda_T}{\partial \zeta}\right) \phi' \end{aligned} \tag{3a}$$

and

$$\begin{aligned} \gamma_{x\eta}^s &= v_s' \cos(\theta_0 + \hat{\phi}) + w_s' \sin(\theta_0 + \hat{\phi}) \\ \gamma_{x\zeta}^s &= w_s' \cos(\theta_0 + \hat{\phi}) - v_s' \sin(\theta_0 + \hat{\phi}) \end{aligned} \tag{3b}$$

where λ_T is the Saint Venant warping function. In the previous expression, for the sake of convenience, shear strain com-

ponents, γ_{ij}, are decomposed into torsion-related engineering strain components, γ^t_{ij}, and transverse-shear-related engineering strain components, γ^s_{ij}. In the case of a box-beam cross section, the warping function λ_T is written as follows[12]:

$$\lambda_T(\eta, \zeta) = \beta\eta\zeta$$
$$\beta = \frac{\mu - 1}{\mu + 1}, \qquad \mu = \frac{b \cdot t_v \cdot G_v}{h \cdot t_h \cdot G_h} \tag{4}$$

where G_h and G_v are respectively effective inplane shear stiffness for horizontal and vertical walls of the box beam.

The stress-strain relations for a composite beam are modified by adding an additional stiffness coefficient corresponding to the transverse shear modulus. In the horizontally laminated plies of the composite box-beam wall, the constitutive relations are in the form

$$\begin{Bmatrix} \sigma_{xx} \\ \sigma_{x\eta} \\ \sigma_{x\zeta} \end{Bmatrix} = \begin{bmatrix} \bar{Q}_{11} & \bar{Q}_{16} & 0 \\ \bar{Q}_{16} & \bar{Q}_{66} & 0 \\ 0 & 0 & \bar{Q}_{55} \end{bmatrix} \begin{Bmatrix} \varepsilon_{xx} \\ \gamma_{x\eta} \\ \gamma_{x\zeta} \end{Bmatrix} \tag{5a}$$

and for the vertical laminae

$$\begin{Bmatrix} \sigma_{xx} \\ \sigma_{x\zeta} \\ \sigma_{x\eta} \end{Bmatrix} = \begin{bmatrix} \bar{Q}_{11} & \bar{Q}_{16} & 0 \\ \bar{Q}_{16} & \bar{Q}_{66} & 0 \\ 0 & 0 & \bar{Q}_{55} \end{bmatrix} \begin{Bmatrix} \varepsilon_{xx} \\ \gamma_{x\zeta} \\ \gamma_{x\eta} \end{Bmatrix} \tag{5b}$$

where the expressions for the transformed reduced stiffness matrix $\bar{Q}_{ij}$ in terms of material constants are given in Jones.[13] A more detailed modeling of two-dimensional inplane elasticity (plane stress assumption) is used to modify the preceding relations as described in Refs. 6 and 12. It was assumed that the distribution of shear strain associated with the transverse shear deformations of the box beam is uniform over the cross section of the beam. But it is recognized that this assumption needs to be modified because the distribution of shear strain (or stress) in the inplane direction of the wall is nearly parabolic, having zero in the free surface of the beam, and the length of the wall is quite large compared with the wall thickness. Therefore we will later introduce the shear correction factors to compensate for this error. It is assumed further that the shear strains $\gamma_{x\zeta}$ in the horizontal plies of the wall and $\gamma_{x\eta}$ in the vertical plies of the wall are composed of the transverse-shear-related components only since the torsional deformation contributes mainly to the shear strain in the other direction.

The governing differential equations of motion for the composite beam can be derived by using Hamilton's principle

$$\int_{t1}^{t2} (\delta U - \delta T - \delta W_e)\, dt = 0 \tag{6}$$

where δU, δT, and δW_e are the variation of strain energy, the variation of kinetic energy, and the virtual work done, respectively, and t is the time period of the motion. Note that, in obtaining the governing variational equations in terms of displacement components, a dimensionless scaling parameter, $m\Omega^2R^2/EA$, which is the ratio of inertial terms to structural terms, was assumed to have the same order of magnitude (ε^2) as that of Ref. 4 for an isotropic rotor. This can also be applied to the composite blade because the composites have high stiffness but low density.

The variation of strain energy for the composite blade is given by

$$\delta U = \int_0^R \int\int_A (\sigma_{xx}\delta\varepsilon_{xx} + \sigma_{x\eta}\delta\gamma_{x\eta} + \sigma_{x\zeta}\delta\gamma_{x\zeta})\, d\eta\, d\zeta\, dx \tag{7}$$

Substituting Eqs. (5a) and (5b) into Eq. (7) and using the notation of the decomposition of the shear strain components, the strain energy expression results in

$$\begin{aligned}\delta U = \int_0^R \Bigg[&\int\int_{A_H} \{(C_{11}\varepsilon_{xx} + C_{16}\gamma^t_{x\eta})\delta\varepsilon_{xx} \\ &+ (C_{16}\varepsilon_{xx} + C_{66}\gamma^t_{x\eta})\delta\gamma^t_{x\eta}\}\, d\eta\, d\zeta \\ &+ \int\int_{A_V} \{(C_{11}\varepsilon_{xx} + C_{16}\gamma^t_{x\zeta})\delta\varepsilon_{xx} + (C_{16}\varepsilon_{xx} \\ &+ C_{66}\gamma^t_{x\zeta})\delta\gamma^t_{x\zeta}\}\, d\eta\, d\zeta \Bigg]\, dx + \int_0^R A\, [\{k_{22}(C_{55} \\ &+ C_{66})\gamma^s_{x\zeta} + k_{12}C_{16}\varepsilon_{xx} + k_{24}C_{66}\gamma^t_{x\zeta}\}\delta\gamma^s_{x\zeta} \\ &+ \{k_{33}(C_{55} + C_{66})\gamma^s_{x\eta} + k_{13}C_{16}\varepsilon_{xx} \\ &+ k_{34}C_{66}\gamma^t_{x\eta}\}\delta\gamma^s_{x\eta} + (k_{12}C_{16}\gamma^s_{x\zeta} + k_{13}C_{16}\gamma^s_{x\eta})\delta\varepsilon_{xx} \\ &+ k_{24}C_{66}\gamma^s_{x\zeta}\delta\gamma^t_{x\zeta} + k_{34}C_{66}\gamma^s_{x\eta}\delta\gamma^t_{x\eta}]\, dx\end{aligned} \tag{8}$$

where the second part of the strain energy expression represents additional strain energy due to transverse shear deformations, A is the cross-sectional area of the box beam, A_H the cross-sectional area of the horizontal wall, and A_V the cross-sectional area of the vertical wall; k_{22} and k_{33} are the shear correction factors, respectively, for flap and lag directions, k_{12} and k_{13} the shear correction factors for bending-shear coupling, and k_{24} and k_{34} the shear correction factors for torsion-shear coupling. The shear correction factors k_{22} and k_{33} are the ones required for Timoshenko's beam theory.[14] The evaluation of shear correction factors, k_{ij}, depends on the exact treatment of the flexure-torsion behavior of the beam. Much work is needed for the evaluation of k_{ij} due to the inherent complexity of the problem, and we do not go further to obtain the solution of k_{ij} at the present time, instead, Cowper's solution[9] of k_{ij} for homogeneous isotropic box section is used to describe the motion (see Appendix). But, to show the validity of using the Cowper's solution, the three-dimensional, finite element analysis of the composite box beam is carried out. The box beam is analyzed by using 1280 HEXA elements of the MSC/NASTRAN with respect to layer angle change. Comparative results for k_{22} are presented in Table 1.[15] It is found that the error between the computed results and Cowper's results is generally within 3–10%. Substituting the strain-displacement relations (3a) and (3b) into the strain energy expression (8), the variational form of the strain energy in terms of displacement components is obtained.

The expression for the kinetic energy is assumed the same for a composite blade as for a metal blade, and the variation of the kinetic energy can be written in the form

$$\delta T = \int_0^R \int\int_A \rho V \cdot \delta V\, d\eta\, d\zeta\, dx \tag{9}$$

Table 1 Calculated shear correction factor using the three-dimensional stress analysis of MSC/NASTRAN

Layer angle (deg)	Shear correction factor
0	0.763
15	0.801
30	0.820
45	0.825
60	0.827
75	0.827
90	0.827
Cowper's[9]	0.738

where V is the velocity vector of a given point on the deformed blade. The variational form of the kinetic energy in terms of displacement components keeping second-degree geometric nonlinearities can be developed using Eq. (9), and can be written as follows

$$\delta T = \int_0^R m \Big[\{\Omega^2 x + 2\Omega(\dot{v}_b + \dot{v}_s) - \ddot{u}\}\delta u + \{\Omega^2(v_b + v_s) - 2\Omega\dot{u} + e_g\Omega^2(\cos\theta_0 - \hat{\phi}\sin\theta_0) + 2\Omega\beta_p(\dot{w}_b + \dot{w}_s) - (\ddot{v}_b + \ddot{v}_s) + 2e_g\Omega(\dot{v}_b'\cos\theta_0 + \dot{w}_s'\sin\theta_0) + e_g\ddot{\hat{\phi}}\sin\theta_0\}\delta v_b + \{\Omega^2(v_b + v_s) + e_g\Omega^2\cos\theta_0 + 2\Omega\beta_p\dot{w}_b - 2\Omega\dot{u} - (\ddot{v}_b + \ddot{v}_s)\}\delta v_s - \{\beta_p\Omega^2 x + 2\beta_p\Omega(\dot{v}_b + \dot{v}_s) + (\ddot{w}_b + \ddot{w}_s) + e_g\ddot{\hat{\phi}}\cos\theta_0\}\delta w_b - \{\beta_p\Omega^2 x + 2\beta_p\Omega\dot{v}_b + (\ddot{w}_b + \ddot{w}_s)\}\delta w_s - \{k_m^2\ddot{\hat{\phi}} + \frac{\Omega^2}{2}(k_{m2}^2 - k_{m1}^2)\sin 2\theta_0 + e_g\Omega^2 x(w_b'\cos\theta_0 - v_b'\sin\theta_0) + e_g\Omega^2 v_b\sin\theta_0 + e_g\Omega^2\beta_p x\sin\theta_0 - e_g(\ddot{v}_b\sin\theta_0 - \ddot{w}_b\cos\theta_0)\}\delta\hat{\phi} - e_g\{\Omega^2(x\cos\theta_0 - \hat{\phi}x\sin\theta_0) + 2\Omega\dot{v}_b\cos\theta_0\}\delta v_b' + k_{m2}^2\ddot{v}_b'\delta v_b' - e_g\{\Omega^2(x\sin\theta_0 + \hat{\phi}x\cos\theta_0) + 2\Omega\dot{v}_b\sin\theta_0\}\delta w_b' + k_{m1}^2\ddot{w}_b'\delta w_b' - e_g\Omega^2 x\cos\theta_0\delta v_s' - e_g\Omega^2 x\sin\theta_0\delta w_s' \Big] dx \tag{10}$$

where e_g is the center of mass offset for the elastic axis.

The virtual work done by the nonconservative aerodynamic forces can be written as

$$\delta W_e = \int_0^R (L_u\delta u + L_v\delta v + L_w\delta w + M_\phi\delta p)\, dx \tag{11}$$

where L_u, L_v, L_w, and M_ϕ are aerodynamic forces distributed along the length of the blade in the axial, lead-lag, flap, and torsion directions, respectively. The δp is the virtual rotation of a point on the deformed elastic axis.[16] The noncirculatory aerodynamic components are included in this variational equation. As the kinetic energy expression, the total transverse displacements of lag and flap directions in Eq. (11) are expressed as the sum of the displacement due to bending and the displacement due to shear deformation.

Damped Element Model

The advanced composite materials show high damping characteristics in the transverse direction but low damping characteristics in the fiber direction, due to the properties of the matrix and the fibers. The damping property should be considered with respect to layer angle change, because the damping of a composite material has a directional nature.[17] The specific damping capacity (SDC), ψ, associated with the flexural response of the beam is defined as[11]:

$$\psi = \frac{\Delta U}{U} \tag{12}$$

where ΔU is the strain energy dissipated during a stress cycle, and U is the total strain energy of the structure. The energy dissipation of the composite beam can be written in the form

$$\Delta U = \frac{1}{2}\int_V \boldsymbol{\varepsilon}^T\boldsymbol{D}^*\boldsymbol{\varepsilon}\, dV \tag{13}$$

where $\boldsymbol{\varepsilon}$ is the strain vector defined in Eq. (2a), the superscript T denotes the transpose of a matrix, and the damped elasticity matrix, $\boldsymbol{D}^*$, is given by

$$\boldsymbol{D}^* = \begin{bmatrix} \bar{Q}_{11}^* & \bar{Q}_{16}^* \\ \bar{Q}_{61}^* & \bar{Q}_{66}^* \end{bmatrix}$$

in which $\bar{Q}_{ij}^*$ can be obtained from the relation as

$$\bar{\boldsymbol{Q}}^* = \boldsymbol{T}^T \operatorname{diag}\{\psi_1 \quad \psi_2 \quad \psi_{12}\}\boldsymbol{Q}\boldsymbol{T}$$

where $\boldsymbol{T}$ is the transformation matrix between the arbitrary coordinate axes and the principal material axes,[13] $\boldsymbol{Q}$ the reduced stiffness matrix,[13] ψ_1, ψ_2, and ψ_{12} are, respectively, the SDC of fiber direction, transverse direction, and inplane shear direction, and the diag{ } the diagonal matrix. These SDCs may be considered as material constants, which can be determined from an elaborate test.[10,11,18] As described in the previous section, a more detailed modeling of two-dimensional inplane elasticity is used to modify the preceding relations. Note that the damped matrix $\bar{Q}_{ij}^*$ is no longer symmetric although $\bar{Q}_{ij}$ is symmetric.

The modal SDC $\bar{\psi}$ is obtained from Eq. (12) through a descretization process described in the following section and a modal transformation, which is written as

$$\bar{\psi} = \frac{\boldsymbol{\Phi}^T\boldsymbol{K}_D\boldsymbol{\Phi}}{\boldsymbol{\Phi}^T\boldsymbol{K}_S\boldsymbol{\Phi}} \tag{14}$$

where $\boldsymbol{K}_S$ and $\boldsymbol{K}_D$ are, respectively, the undamped and the damped stiffness matrices, and $\boldsymbol{\Phi}$ is the modal matrix calculated from the undamped free vibration analysis of the nonrotating beam. The damped stiffness matrix can be obtained from the dissipated energy equation (13). The ith modal SDC, with respect to the ith mode shape vector $\{\phi\}_i$, can be determined from Eq. (14). As a result, the modal damping matrix can be obtained from the modal SDC as follows:

$$\bar{\boldsymbol{C}}_d^* = \operatorname{diag}\{2\zeta_1\omega_1 \quad 2\zeta_2\omega_2 \ldots 2\zeta_i\omega_i\} \tag{15}$$

where the ith damping ratio ζ_i is the ith modal SDC $\bar{\psi}_i$ divided by 2π.

Finite Element Discretization

The blade is divided into a series of beam elements. Each element consists of two end nodes and three internal nodes, which results in a total of 23 DOF including eight transverse shear degrees of freedom. The element has 10 DOF at each of the two end nodes; the deflections due to bending, v_b and w_b, the deflections due to shear, v_s and w_s, and their derivatives with respect to x, the axial displacement u, and the twist angle $\hat{\phi}$. Among the three internal nodes, two are for u and one is for $\hat{\phi}$. The torsional degree of freedom $\hat{\phi}$, instead of ϕ, is used in the present analysis to keep the banded character of the system matrices.[19]

The Hamilton's principle given in Eq. (6) is discretized as

$$\int_{t1}^{t2}\sum_{i=1}^{N_e}(\delta U_i - \delta T_i - \delta W_{ei})\, dt = 0 \tag{16}$$

where N_e is the total number of finite elements, and the subscript i represents the contribution of an ith element. The final nonlinear equations of motion in terms of nodal degrees of freedom $\boldsymbol{q}$ are obtained by using the preceding equation (16), which results in

$$\boldsymbol{M}(\boldsymbol{q})\ddot{\boldsymbol{q}} + \boldsymbol{C}(\boldsymbol{q})\dot{\boldsymbol{q}} + \boldsymbol{K}(\boldsymbol{q})\boldsymbol{q} = \boldsymbol{F} \tag{17}$$

where $\boldsymbol{M}$, $\boldsymbol{C}$, $\boldsymbol{K}$, and $\boldsymbol{F}$ are the global inertia, damping, stiffness matrices, and load vector, respectively.

Solution Procedure

The first step in solving Eq. (17) is to get the steady trim solution. The blade steady-state equations are obtained by neglecting all time-dependent terms in the governing equation (17). The nonlinear trimmed states of the blade are calculated iteratively by using the standard Newton-Raphson technique, which generally guarantees quadratic convergence, and several iteration steps are performed to insure the accuracy of the solutions. In the next stage, the free vibration analysis of the rotating blade about the equilibrium position is conducted to determine the natural modes. A modal coordinate transformation based on these normal modes is then performed to reconstruct the system inertia, damping, and stiffness matrices. To consider the low-frequency unsteady aerodynamic effects in the following stability analysis, a simple dynamic inflow model for hover is used as[7]:

$$\frac{128}{75\pi}\delta\dot{\lambda} + 4\lambda_{i0}\delta\lambda = \frac{1}{\rho_a \pi R^2 (R\Omega)^2}\sum_{i=1}^{N_b}\int_0^R \delta L_{w_c}\,dx \qquad (18)$$

where λ_{i0} is the mean induced inflow ratio, $\delta\lambda$ the perturbation inflow component, ρ_a the air density, N_b the total number of blades, and L_{w_c} the circulatory aerodynamic force acting on the blade in the flapwise direction. The resulting flutter equations of motion, which include the information for dynamic inflow and structural damping, can be written in the following form

$$\bar{M}_\lambda \ddot{r}_\lambda + (\bar{C}_d^* + \bar{C}_\lambda)\dot{r}_\lambda + \bar{K}_\lambda r_\lambda = \mathbf{0} \qquad (19)$$

where the bars over the matrices indicate that these matrices have been evaluated using the modal coordinate transformation, $\bar{C}_d^*$ is the modal damping matrix defined in Eq. (15), and r the modal coordinates. An additional degree of freedom, λ, is included in this modal flutter equation to take into account the dynamic inflow effects. Finally, the stability analysis of the blade is conducted from the self-exited instability equation (19), which is to be transformed into a first-order system and solved as an algebraic eigenvalue problem.

Results and Discussion

Comparison of Results for Rotating Composite Box Beams

Numerical simulations for the structural dynamic behavior of rotating composite box beams are carried out to correlate the current approach with the existing alternative solutions. The comparison is conducted for both symmetric and antisymmetric layup beams. In the symmetric configuration, the side laminates have $[\Lambda_V/-\Lambda_V]_3$ whereas the top and bottom laminates have $[\Lambda_H]_6$. For the antisymmetric configuration, the top and left laminates have $[0/\Lambda_H$ or $\Lambda_V]_3$ whereas the ply layups on opposite laminates have reversed orientation. Positive ply angles for the horizontal (Λ_H) and the vertical (Λ_V) laminates are defined in Fig. 1. The length, R, of the beam is 0.845 m and the outer dimension of the box section is 0.0242 m × 0.0136 m. The mechanical properties used were those of AS4/3501-6 graphite epoxy[6]: E_{11} = 141.9 GPa, E_{22} = 9.790 GPa, $G_{12} = G_{13}$ = 6.134 GPa, ν_{12} = 0.42, and ρ = 1445 kg/m^3. The shear correction factors for flap and lag directions of the beam are calculated using the equation (A1), and they are: k_{22} = 0.2773, k_{33} = 0.6030; the rest are: $k_{12} = k_{13}$ = 1, and $k_{24} = k_{34}$ = 0.

Figures 2 and 3 show the comparison of natural frequencies for the three fundamental modes (two flap and one lag), respectively, for symmetric (Fig. 2) and antisymmetric (Fig. 3) layups of the rotating box beam, obtained using the current approach, and that of Smith and Chopra.[6] The experimental data used in the comparison is taken from Chandra and Chopra.[20] Results from the present analysis were obtained using six spanwise (shear-flexible) beam elements. It is shown in the figures that, through different kinds of laminate configurations, the present results are in good agreement with those of experimental data, especially in the case of antisymmetric layups, and generally more accurate than those of Ref. 6. It is presented that the differences between the results of current work and those of Ref. 6 can mainly be attributed to the use of shear correction factors, because the results of Ref. 9 are almost identical to those without shear correction. Note that, for both symmetric and antisymmetric layups, the effect of the shear correction factor on the lower modes is not significant, but the effect on the higher modes becomes notable, as seen in the two plots.

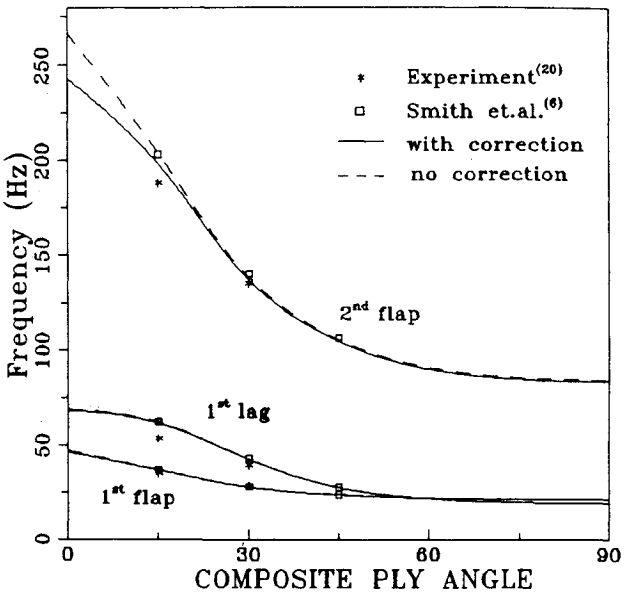

Fig. 2 Comparison of rotating natural frequencies of the box beam in symmetric layups.

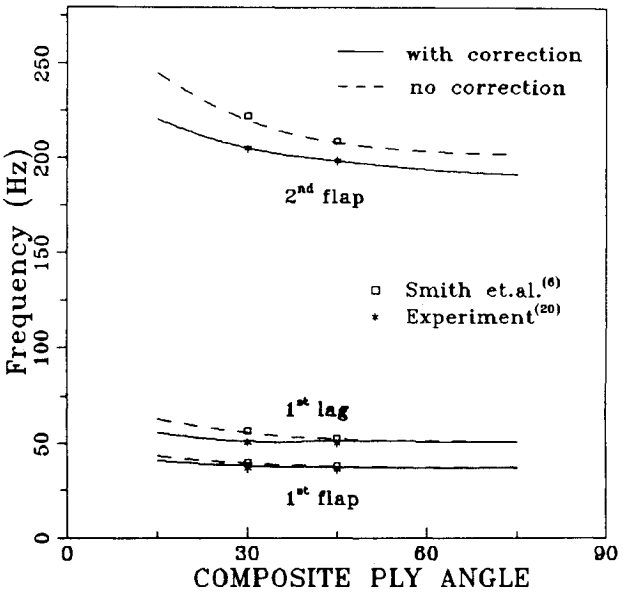

Fig. 3 Comparison of rotating natural frequencies of the box beam in antisymmetric layups.

Figure 4 shows the influence of rotational speed on the calculated and the experimental values of the first three fundamental frequencies (first two flap and first lag) for $[30]_6$ symmetric graphite-epoxy beams. The test results are obtained from Ref. 20. A good correlation between these two results is seen clearly in the plot.

Influence of Transverse Shear on the Aeroelastic Response

Numerical results are obtained for a hingeless rotor blade with Lock number γ = 5.0, solidity ratio σ = 0.1, chord to

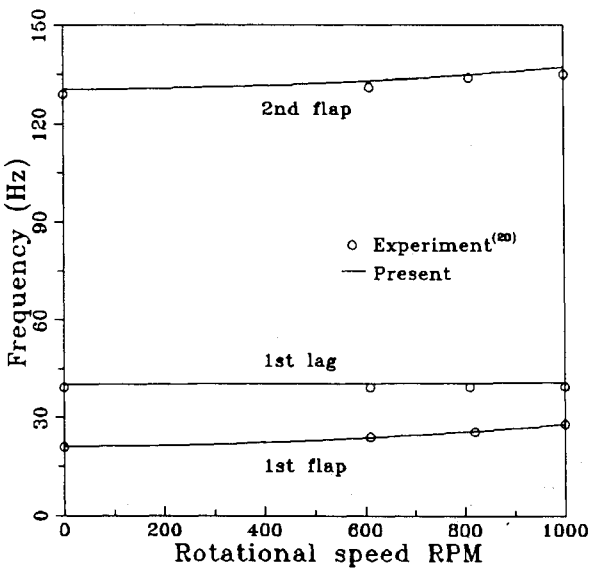

Fig. 4 Comparison of natural frequencies of a graphite-epoxy box beam in symmetric layups with $[30]_6$ in top and bottom laminates and $[30/-30]_3$ in vertical laminates at various rotational speeds.

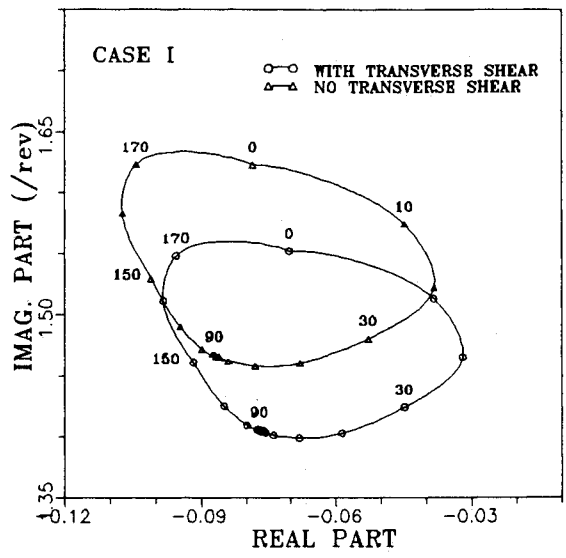

Fig. 5 Effect of transverse shear on the stability solution of the first lag mode (case I).

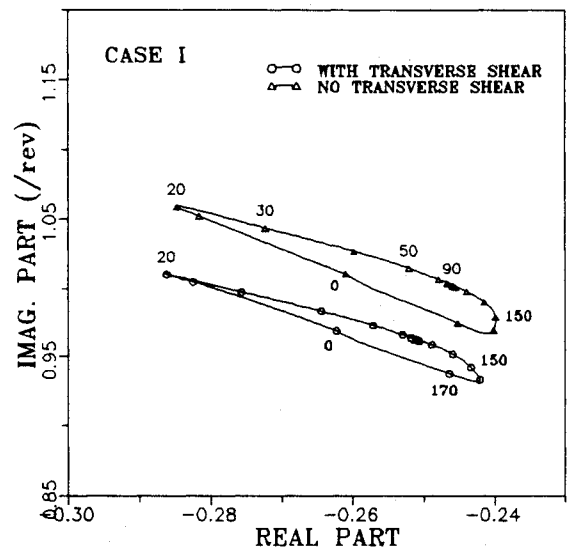

Fig. 6 Effect of transverse shear on the stability solution of the first flap mode (case I).

span ratio $c/R = 0.08$, and zero precone. The chordwise offsets of the center of mass, aerodynamic center, and tension center from the elastic axis are assumed to be zero. The airfoil characteristics used were: $c_l = 5.7\alpha$, $c_d = 0.01$, and $c_{\text{mac}} = 0$. The blade structure is represented by a laminated composite box beam. Five normal modes (two flap, two lag, and one torsion) calculated at the deformed equilibrium position of the blade are used to perform the stability analysis. A baseline blade configuration with zero ply angles on all four laminates of the box beam has a stiff inplane property as: the first flap frequency $\omega_w = 1.15$/rev, the first lag frequency $\omega_\zeta = 1.5$/rev, and the first torsion frequency $\omega_\phi = 5.0$. Two different ply configurations (denoted as case I and case II) are considered in the calculation. In case I, the horizontal laminae have zero ply angles, while the laminae in the outer half of the vertical walls have zero ply angles and the laminae in the inner half walls are all oriented at the same layer angle Λ_V. In the case II configuration, the vertical laminae have zero angles, while the laminae in the outer half of the horizontal walls have zero angles and the laminae in the inner half walls are all oriented at the same layer angle Λ_H. These lamination configurations are chosen simply to show the effect of transverse shear deformations on the dynamic behavior of the rotor with changing ply angles. The length, R, of the rotor is 4.42 m and the cross section of the beam has an outside dimension of 0.178 m width by 0.051 m height with 8.89×10^{-3} m thick. The elastic material properties used were $E_{11} = 206.7$ GPa, $E_{22} = 20.67$ GPa, $G_{12} = G_{13} = 8.270$ GPa, $\nu_{12} = 0.3$, and $\rho = 1742$ kg/m^3. The calculated shear correction factors in this model are: $k_{22} = 0.1264$ and $k_{33} = 0.7377$, and the others are assumed to be zero.

Figures 5 and 6 show the root locus plots of complex eigenvalues vs fiber angle Λ_V for the first lag and flap modes, respectively, at a thrust level of $C_T/\sigma = 0.1$ (case I), as the layer angle is varied from 0 to 180 deg. The layer angles, Λ_V, of 0 and 180 deg yield the same ply configuration, with fibers oriented parallel to the blade axis on the side wall of the beam. Figure 5 shows that the ply angle change has a considerable influence on the blade lag mode stability. The maximum damping value is obtained at about 160 deg of the layer angle for this configuration. The effect of transverse shear on the stability solution for this lag mode is shown in the plot to be quite substantial. With the inclusion of transverse shear, there is a large decrease in the frequency and damping of the lag mode; that is, the transverse shear flexibility softens the lag mode and destabilizes the motion. There is also a considerable influence of the change of ply angle Λ_V on the first flap mode as presented in Fig. 6. It is found in the plot that transverse shear tends to lower the frequency of the blade, with a slight increase in flap mode damping. The behavior of torsion mode is not changed by the inclusion of transverse shear flexibility and is not shown.

Figures 7 and 8 show the root locus plots with changing ply angle Λ_H for the first lag and flap modes, respectively, at a thrust level of $C_T/\sigma = 0.1$ (case II). The influence of transverse shear on the lag mode stability is appreciable on both the frequency as well as the damping of the mode as shown in Fig. 7. The transverse shear reduces the lag mode frequency and decreases damping as in the case I configuration. The influence of Λ_H on the flap mode frequency is quite large as presented in Fig. 8. Positive Λ_H (0 deg $< \Lambda_H <$ 90 deg) stiffens the flap mode and negative Λ_H (90 deg $< \Lambda_H <$ 180 deg) softens the flap mode. Very low flap frequency of the blade is obtained for Λ_H of 160–170 deg. The blade seems to meet a critical flapping state at these ply angles. Similar statements were also dipicted in Ref. 3. The effect of transverse shear on the flap mode is again quite significant. At layer angles Λ_H of 0–130 deg, the transverse shear tends to stabilize the motion as in the previous case I result. The effect of transverse shear, however, is reversed at Λ_H of 150–170 deg. This fact

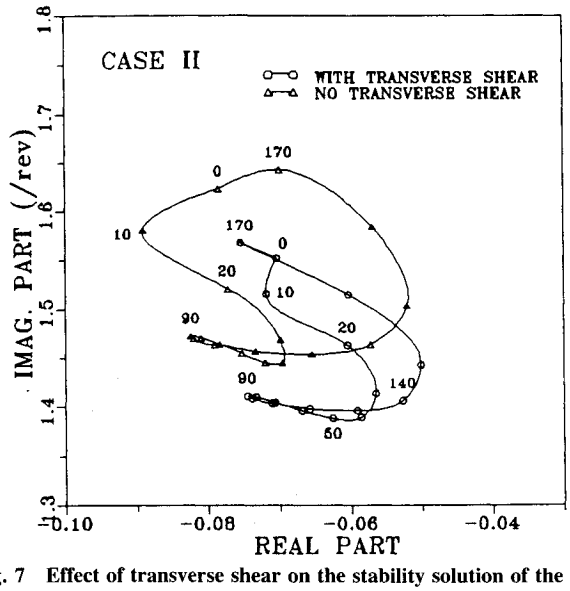

Fig. 7 Effect of transverse shear on the stability solution of the first lag mode (case II).

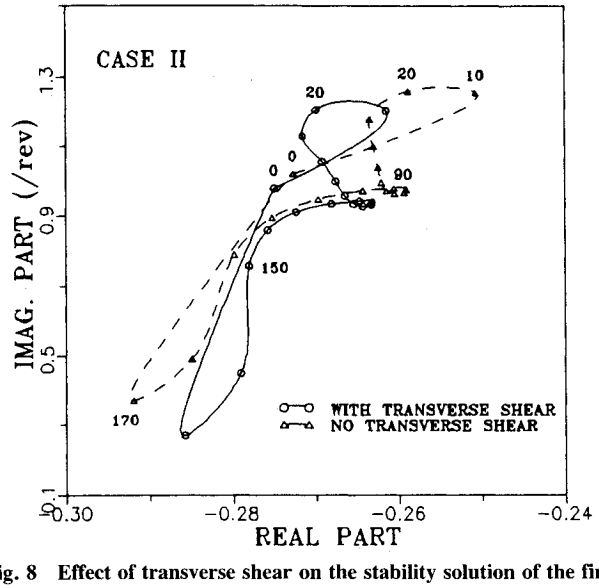

Fig. 8 Effect of transverse shear on the stability solution of the first flap mode (case II).

is thought to be in close relation with the previously mentioned critical flapping condition.

Influence of Structural Damping for Composite Box Beams

The variation of the first four natural frequencies (two flap and two lag) and the modal damping ratios with fiber orientation are presented in Fig. 9. The elastic material properties and the specific damping capacities used in the calculation were those of HMS/DX-210 carbon epoxy[18]: E_{11} = 172.6 GPa, E_{22} = 7.168 GPa, G_{12} = G_{13} = 3.791 GPa, ν_{12} = 0.291, ψ_1 = 0.0045, ψ_2 = 0.042, and ψ_{12} = 0.0705. The physical dimensions and the lamination details (symmetric layup) used in the calculation are the same as those given earlier in the comparison study. The calculated damping ratios and the natural frequencies of the box beam show opposite trends from each other as seen in Fig. 9. This is explained by the fact that the ply orientation with higher stiffness would produce less energy dissipation resulting in lower values of damping ratio than the ply orientation with lower stiffness. It is noted that a similar statement on the variation of moduli and damping with fiber orientation can also be found in Ni and Adams.[18] The results shown in Fig. 9 indicate that both the natural frequency and inherent structural damping can be controlled altogether by a composite tailoring technique.

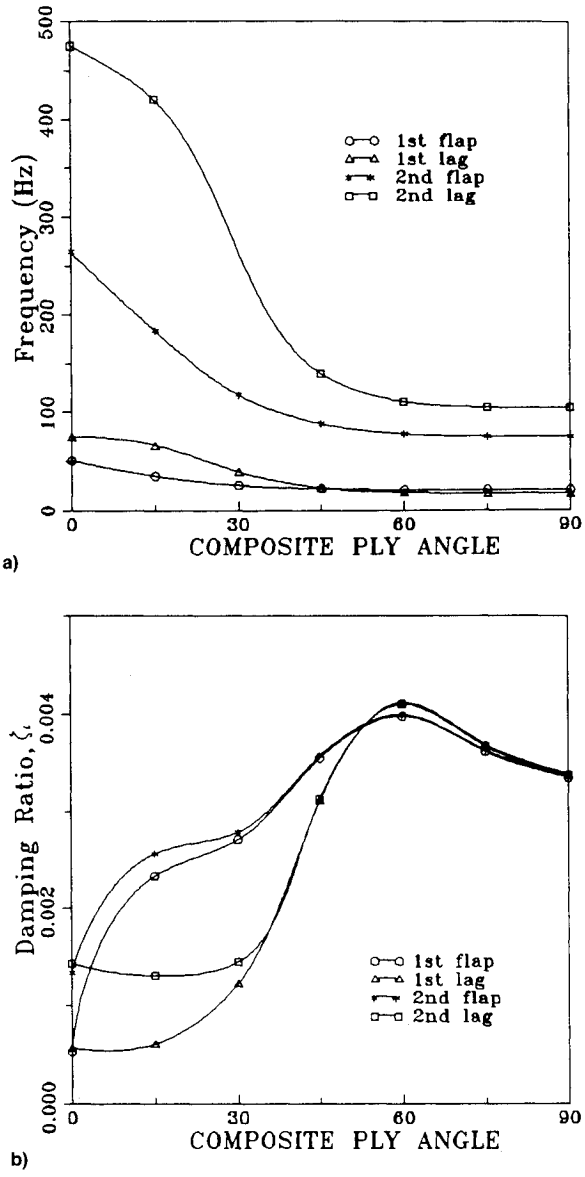

Fig. 9 Variation of frequency and damping with respect to layer angle for a HMS/DX-210 carbon-epoxy box beam: a) frequency and b) damping.

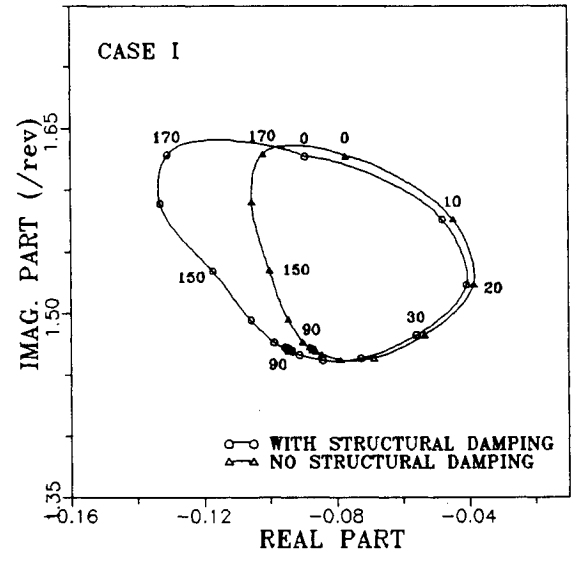

Fig. 10 Effect of structural damping on the stability solution of the first lag mode (case I).

Figure 10 demonstrates the effect of structural damping on the first lag mode of the composite rotor with changing ply angle Λ_V. The aforementioned case I configuration with the material properties of specific damping capacity in HMS/DX-210 carbon-epoxy lamina was used to obtain the quantitative values of structural damping. The structural damping incorporated in the analysis has a stabilizing effect on the system's aeroelastic behavior as was expected. One also notices in the plot that quite a large amount of positive damping is to be generated at the layer angles Λ_V of 130–170 deg.

Conclusion

A finite element analysis used to incorporate the effects of transverse shear deformations and structural damping on the aeroelastic behavior of composite rotor blades in hover has been presented. Based on the present work, the following conclusions can be drawn.

1) Despite the simplified assumptions made in the determination of shear correction factors, the present beam model provided realistic solutions in the structural dynamic analysis compared with experimental data. Therefore, this approach of shear correction factors in the analysis of a composite rotor furnishes a convenient alternative to the formulation of the blade with transverse shear deformations.

2) The effects of transverse shear on the aeroelastic behavior of the composite rotor may be quite substantial in that they stabilize or destabilize the motion somewhat; thus the transverse shear flexibility should be kept for the analysis to get more enhanced results.

3) The damping capacities of the composite laminates can be increased by changing ply orientation angle, i.e., a tailoring technique can be utilized in the area of structural damping to perform more refined aeroelastic analysis of a composite rotor blade.

Appendix: Shear Correction Factor

The shear correction factor k_{22} (flapwise) for the isotropic thin-walled box section is obtained from a three-dimensional elasticity approach, and is given as[9]:

$$k_{22} = \frac{10(1 + \nu_{12})(1 + 3r)^2}{f_1 + \nu_{12} f_2 + 30rs^2(1 + r) + 5\nu_{12} rs^2(8 + 9r)} \tag{A1}$$

$$f_1 = 12 + 72r + 150r^2 + 90r^3$$

$$f_2 = 11 + 66r + 135r^2 + 90r^3$$

where r is bt_h/ht_v and sb/h. Note that the shear correction factor in the other direction (lagwise) is determined by the preceding equation through the inversion of r and s.

References

[1]Rehfield, L. W., Atilgan, A. R., and Hodges, D. H., "Nonclassical Behavior of Thin-Walled Composite Beams with Closed Cross Sections," *Journal of the American Helicopter Society*, Vol. 35, No. 2, 1990, pp. 42–50.

[2]Kapania, R. K., and Raciti, S., "Nonlinear Vibrations of Unsymmetrically Laminated Beams," *AIAA Journal*, Vol. 27, No. 2, 1989, pp. 201–210.

[3]Hong, C. H., and Chopra, I., "Aeroelastic Stability Analysis of a Composite Rotor Blade," *Journal of the American Helicopter Society*, Vol. 30, No. 2, 1985, pp. 57–67.

[4]Hodges, D. H., and Dowell, E. H., "Nonlinear Equations of Motion for the Elastic Bending and Torsion of Twisted Nonuniform Blades," NASA TN D-7818, Dec. 1974.

[5]Rand, O., "Periodic Response of Thin-Walled Composite Helicopter Rotor Blades," *Journal of the American Helicopter Society*, Vol. 36, No. 4, 1991, pp. 3–11.

[6]Smith, E. C., and Chopra, I., "Aeroelastic Response and Blade Loads of a Composite Rotor in Forward Flight," *Proceedings of the 33rd AIAA/ASME/ASCE/ASC Structures, Structural Dynamics, and Materials Conference*, AIAA, Washington, DC, 1992, pp. 1996–2014 (AIAA Paper 92-2466).

[7]Pitt, D. M., and Peters, D. A., "Theoretical Prediction of Dynamic Inflow Derivatives," *Vertica*, Vol. 5, No. 1, 1981, pp. 21–34.

[8]Chen, A. T., and Yang, T. Y., "Static and Dynamic Formulation of a Symmetrically Laminated Beam Finite Element for a Microcomputer," *Journal of Composite Materials*, Vol. 19, Sept. 1985, pp. 459–475.

[9]Cowper, G. R., "The Shear Coefficient in Timoshenko's Beam Theory," *Journal of Applied Mechanics*, June 1966, pp. 335–340.

[10]Koo, K. N., and Lee, I., "Finite Element Analysis of Vibration and Damping for Symmetric Composite Laminates," *Proceedings of the Eighth International Conference on Composite Materials (ICCM/8)* (Honolulu, Hawaii), July 1991, pp. 34-C, 1-10.

[11]Lin, D. X., Ni, R. G., and Adams, R. D., "Prediction and Measurement of the Vibrational Damping Parameters of Carbon and Glass Fibre-Reinforced Plastics Plates," *Journal of Composite Materials*, Vol. 18, March 1984, pp. 132–152.

[12]Smith, E. C., and Chopra, I., "Formulation and Evaluation of an Analytical Model for Composite Box-Beams," *Journal of the American Helicopter Society*, Vol. 36, No. 3, 1991, pp. 23–35.

[13]Jones, R. M., *Mechanics of Composite Materials*, McGraw-Hill, Washington, DC, 1975, Chap. 2.

[14]Timoshenko, S. P., "On the Correction for Shear of the Differential Equations for Transverse Vibrations of Prismatic Beams," *Philosophical Magazine*, Vol. 41, No. 8, 1921, pp. 744–746.

[15]Jung, S. N., Yoon, K. W., and Kim, S. J., "Dynamic Behavior of Rotating Composite Box Beams Considering Transverse Shear Effects," *Journal of Composite Materials* (submitted for publication).

[16]Hodges, D. H., Ormiston, R. A., and Peters, D. A., "On the Nonlinear Deformation Geometry of Euler-Bernoulli Beams," NASA TP-1566, April 1980.

[17]Liao, D. X., Sung, C. K., and Thompson, B. S., "The Optimal Design of Symmetric Laminated Beams Considering Damping," *Journal of Composite Materials*, Vol. 20, Sept. 1986, pp. 485–501.

[18]Ni, R. G., and Adams, R. D., "The Damping and Dynamic Moduli of Symmetric Laminated Composite Beams—Theoretical and Experimental Results," *Journal of Composite Materials*, Vol. 18, March 1984, pp. 104–121.

[19]Sivaneri, N. T., and Chopra, I., "Dynamic Stability of a Rotor Blade Using Finite Element Analysis," *AIAA Journal*, Vol. 20, No. 5, 1982, pp. 716–723.

[20]Chandra, R., and Chopra, I., "Experimental and Theoretical Analysis of Composite I-Beams with Elastic Couplings," *AIAA Journal*, Vol. 29, No. 12, 1991, pp. 2197–2206.